Advances in Water Resources 56 (2013) 77–89

Contents lists available at SciVerse ScienceDirect

Advances in Water Resources

journal homepage: www.elsevier.com/locate/advwatres

# Evaluation of distributed hydrologic impacts of temperature-index and energy-based snow models

Mukesh Kumar [a,*], Danny Marks [b], Jeff Dozier [c], Michele Reba [d], Adam Winstral [b]

[a] Nicholas School of Environment, Duke University, Durham, NC 27708, USA
[b] USDA-ARS Northwest Watershed Research Center, Boise, ID 83712-7716, USA
[c] Bren School of Environmental Science and Management, University of California, Santa Barbara, CA 93106-5132, USA
[d] USDA-ARS National Sedimentation Laboratory, Jonesboro, AR 72401, USA

ARTICLE INFO

*Article history:*
Received 28 September 2012
Received in revised form 8 March 2013
Accepted 13 March 2013
Available online 26 March 2013

*Keywords:*
Snow
Energy-balance
Temperature-index
Hydrologic model

ABSTRACT

Two commonly used strategies in modeling snowmelt are the energy balance and temperature-index methods. Here we evaluate the distributed hydrologic impacts of these two different snowmelt modeling strategies, each in conjunction with a physics-based hydrologic model (PIHM). Results illustrate that both the Isnobal energy-balance and calibrated temperature-index methods adequately reproduce snow depletion at the observation site. However, the models exhibit marked differences in the distribution of snowmelt. When combined with PIHM, both models capture streamflow reasonably during calibration year (WY06), but Isnobal model gives better streamflow results in the validation year (WY07). The uncalibrated temperature-index model predicts streamflow poorly in both years. Differences between distributed snowmelt, as predicted by Isnobal and calibrated temperature-index method, and its consequent effect on predicted hydrologic states suggest the need to carefully calibrate temperature-index models in both time and space. Combined physics-based snow and hydrologic models provide the best accuracy, while a temperature-index model using coefficients from the literature the poorest.



## 1. Introduction

In the mountains of western North America, snowmelt supplies most of the water that supports streamflow and recharge to aquifers. Snow and snowmelt also control the temporal and spatial distributions of soil moisture, evapotranspiration, recharge, streamflow, stream-aquifer interactions, and other hydrologic processes [1,2]. Prediction of accumulation, distribution and melt of snow and associated hydrologic processes are affected by variations in terrain, vegetation, soils, geology, and climate within mountain watersheds. The heterogeneous processes and properties limit our ability to predict seasonal and paroxysmal runoff from these watersheds and therefore limit our choices in managing the water [3].

Among the challenges to understanding and predicting hydrologic interactions in mountain watersheds are the spatio-temporal analyses of snow accumulation and melt. The primary controls on snow accumulation are topography, wind speed and direction, and vegetation. Interaction between these parameters leads to non-uniform spatial distributions that influence both the timing and magnitude of snowmelt across the basin [4]. In a mountain basin, accumulation and melt of seasonal snow varies with elevation, gradient, and radiation exposure [5]. Topography and wind interact to create scour sites on wind-exposed areas and drift zones in their lee [1]. Spatial and temporal distributions of net solar radiation drive the timing and magnitude of snowmelt [6]. Snow redistribution and melt are also influenced by physiographic properties such as soils and protruding rocks within patchy snow, thereby enhancing turbulent and radiative fluxes [7]. Vegetation intercepts snowfall, alters the snow/atmosphere energy exchange and reduces wind speed. Dense canopies tend to reduce snow deposition while sparse canopies enhance it [8]. Snow albedo below forest canopies is lower than that in open snow fields [9] and is subject to a premelt decay caused by deposited leaf litter [10]. In dense forests, trees shade the snow from solar radiation, and longwave radiation becomes the dominant energy source [8]. In general, because of the reduction of wind speed and solar radiation, snow below a forest canopy melts later than in the open.

Snowmelt models usually use one of the following methods: equations in energy-balance (EB) models govern energy and mass conservation for the accumulated snow and are solved together to obtain residual melt, while temperature-index (TI) approaches estimate melt using an empirical relationship with air temperature. Both methods have been used extensively in varied settings. The main advantages of temperature-index method are its

* Corresponding author.
*E-mail addresses:* mukesh.kumar@duke.edu (M. Kumar), ars.danny@gmail.com (D. Marks), dozier@bren.ucsb.edu (J. Dozier), michele.reba@ars.usda.gov (M. Reba), adam.winstral@ars.usda.gov (A. Winstral).

0309-1708/$ - see front matter © 2013 Elsevier Ltd. All rights reserved.
http://dx.doi.org/10.1016/j.advwatres.2013.03.006

simplicity, wide-availability of air temperature data and the computational efficiency in calibration and simulation. The method has been shown to be generally sufficient for prediction of snow accumulation and melt, particularly for open sites [11–13], and has been typically used for operational predictions [14–16].

Energy-balance snow models—such as SNTHERM [17], SnowModel [18], SHAW [19], UEB [20], Isnobal [21], and SNOWPACK [22,23]—have also been widely applied with varying degrees of success. They have been applied either in a semi-distributed manner, by representing the topographic structure as a series of subwatershed hydrologic response units (SNTHERM, SHAW, UEB), or are fully distributed at the resolution of a digital elevation model (SnowModel, Isnobal, SNOWPACK). Energy-balance snow models can include computation of spatial distribution of melt, aspects of snow structure development, and interactions with vegetation and soils.

In this paper we calculate snowmelt by an energy-balance model (Isnobal) and calibrated and uncalibrated temperature index models, and from these we quantify consequent hydrologic impacts. We couple both methods for calculating melt with a distributed hydrologic model, PIHM [24], to address the following four questions: (a) Are distributed snow accumulation and melt calculations in different land covers sensitive to the choice of the modeling approach? (b) How does the selected snowmelt strategy affect streamflow prediction at the watershed outlet? (c) How does the snow modeling approach impact the predicted distribution, timing and magnitude of soil moisture, groundwater, and evapotranspiration? (d) How is the annual water balance for the watershed affected by the selected snow modeling approach?

## 2. Approach

Three model configurations are considered for comparisons. First, Isnobal and PIHM (Is+P) are linked together to simulate surface and subsurface hydrologic processes in a snow-dominated mountain basin. Integrated model simulation from this linkage is then compared to temperature-index snow simulations built into PIHM (Ti+P). Two different Ti+P configurations are used. One uses uncalibrated coefficients from the literature (uncalTi+P) and the other uses calibrated site-specific coefficients developed from local measurements (calTi+P). All three model configurations use a heterogeneous distribution of climate and snow forcings. In the following sections we summarize how the snow modeling approaches, the linking strategy, and details of the hydrologic model configurations are applied over the Reynolds Creek Experimental Watershed (RCEW) in southwestern Idaho.

### 2.1. Snowmelt and distribution model: Isnobal

Isnobal [6,21] solves the snow energy- and mass-balance at each grid cell over a digital elevation model. The model uses a two-layer representation of the snowpack and can be applied to regions with limited data on meteorology, snow structure and temperature. Requiring no calibration, Isnobal has successfully simulated the development and melting of seasonal snow over the Marmot Creek basin in Southwestern Canada [25], the Pacific Northwest [26], the Boise River Basin [27], the Wasatch Range in Utah [28], the sub-Arctic and boreal forest [8], a shrub-covered bog in Northern Canada [29], the California Sierra Nevada [6,30], the central Rocky Mountains [31], and the Reynolds Creek Experimental Watershed [32,33]. It is to be noted that across all these simulations, the independent parameters of Isnobal model are kept the same. The model is driven by meteorological forcing inputs of precipitation, air temperature, incoming shortwave and longwave radiation, wind speed and relative humidity. Forcing data are distributed across the landscape [27,28,30,34]. The model computes water vapor exchange (sublimation or condensation) between snow and atmosphere, and solves for the temperature and snow water equivalent for each layer at each time step. Melt is computed in either layer when its temperature reaches the melting point (0 °C) and more energy is added. Rain produces either water input at the soil surface or adds liquid water and advected energy to the snow. Water drains from the base of the snowpack when the accumulated melt and liquid water content exceed a specified threshold. The model readjusts the snow mass, thickness, thermal properties and measurement heights for both layers after each time-step. The model does not consider interception storage of snow in the canopy. Snow redistribution is computed using information about topography, wind, and precipitation [35]. Before each time-step, snow is redistributed to adjust the snow volume for the formation of drifts and scour zones [36].

### 2.2. Spatially distributed hydrologic model: PIHM

We use the Penn State Integrated Hydrology Model (PIHM) to simulate six hydrologic states over the watershed: snow water equivalent, overland flow, soil moisture of the surface layer, unsaturated zone soil moisture, groundwater depth and stream stage [24,37]. PIHM employs a semi-discrete, finite-volume approach to define the process equations on discretized unit elements, thereby ensuring conservation of the solution property within each. Processes simulated include snowmelt, transpiration, evaporation, overland flow, subsurface flow, streamflow, macropore-based infiltration and lateral stormflow. Streamflow is based on a depth-averaged 1-D diffusive wave equation, surface flow uses a depth-averaged 2-D diffusive wave approximation of the Saint Venant equations, and subsurface flow is based on the depth-averaged, moving boundary approximation of Richards's equation [24]. The model fully couples different physical process states based on the continuity of head and flux. An integrated GIS framework, PIHMgis [38], facilitates automated generation of model input files using geodatabases. An adaptive time-step balances the demands of computational efficiency, accuracy and stability of the solution.

### 2.3. Linked Isnobal–PIHM

Isnobal and PIHM are linked using a one-way coupling strategy, by deactivating the temperature-index snowmelt utility in PIHM, and instead using the snowmelt/surface water output from Isnobal as a flux boundary condition on the PIHM kernel. Ground evaporation in PIHM is shut off at locations covered by snow. Energy exchanges at snow-free locations remain the same. Since Isnobal calculates melt and accumulation only on the ground, interception of snow by vegetation and interception loss is not considered in this paper. However, interception of snow in RCEW is generally limited by the sparse canopy and typical weather that allows the snow to slough from the canopy shortly after deposition. The one-way coupling adds a further simplification in that the ground heat flux does not change with variations in soil moisture. Accounting for ground heat flux is important while the snow accumulates, but once the snowpack is deep, heat flow from the soil is small except in areas of geothermal flux [30,31]. At higher latitudes, ground heat flux and frozen soil conditions before the snow falls are important in the development of the snow's thermodynamic state, but can be neglected in this analysis.

Since Isnobal is raster-based while PIHM simulates the hydrologic states on an unstructured mesh, a transfer utility was developed to move data between raster and mesh representations while ensuring the mass balance. For this experiment, the Isnobal model was run at an hourly time-step and at $10 \times 10$ m spatial resolution. The raster output was then translated to the unstructured mesh,

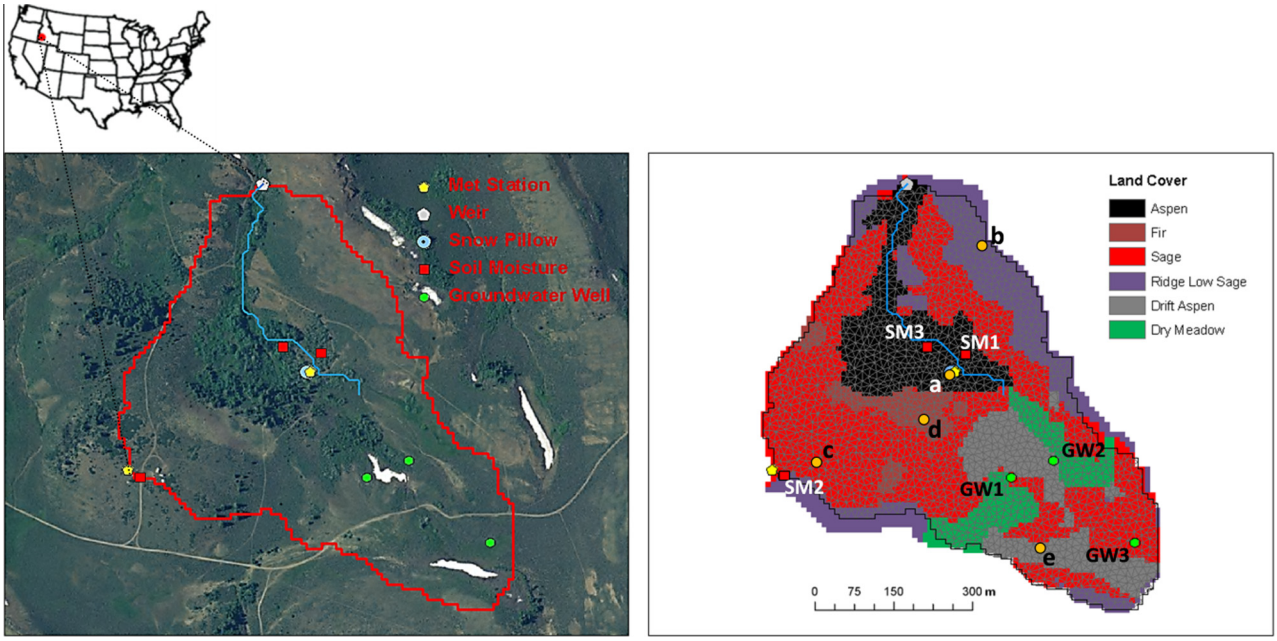


**Fig. 1.** Location of stream gage, snow pillow, groundwater well, soil moisture and meteorological stations (left) in Reynolds' Mountain East (RME) Experimental Watershed. Also shown is the land cover map and domain discretization of the watershed (right) into 3939 prismatic elements and 49 stream elements.

which also has an average resolution of 100 $m^2$, to force the PIHM simulation.

### 2.4. Linked temperature index-PIHM

Impacts due to different characterization of the snow accumulation and melt are explored by comparing watershed response from Is+P simulations to the temperature index included in PIHM (Ti+P), where melt rate is a product of melt factor (MF) and positive air temperature [24]. The Ti+P linked model simulation is driven using the same heterogeneously distributed meteorological datasets that we use in Is+P configuration. Two Ti+P configurations with different melt factors are used. One configuration (uncalTi+P) uses melt factors from SNOW-17, the National Weather Service River Forecasting System (NWRFS) Snow Accumulation and Ablation Model [16], while melt factors in calTi+P are calibrated against snow water equivalent (SWE) measurements from a local snow pillow (Fig. 1).

## 3. Study area: topography, vegetation, soil, geology and climate

We perform the simulations over the Reynolds Mountain East (RME) Watershed, which is a headwater catchment within the Reynolds Creek Experimental Watershed (RCEW) in southwestern Idaho (Fig. 1). RCEW, operated by the US Department of Agriculture, has functioned as a field laboratory for hydrologic research since 1960 [39–41]. The RME watershed is 0.39 $km^2$ in area, elevation ranges from 2027 to 2137 m, and average slope is 8.2°.

About 32% of the RME catchment is forested (split between aspen and mixed conifers) with the remainder of the basin consisting of dry meadow and mixed sagebrush. The watershed can be classified into six land-cover classes (Table 1).

Soils in the watershed range from loam to clay with widely varying coarse fragments. The soils under the forested areas or in the meadow are generally of higher permeability and porosity, whereas those under sage are of lower permeability. We apply a GIS soil layer, with a distribution nearly identical to the GIS vegetation layer [33], in the three simulations. Distributed hydrogeological properties such as porosity, conductivity, anisotropy and moisture-conductivity relationships are not well defined. Eco-geophysical imaging of the subsurface patterns [42] suggests a close relation between geological spatial distribution and that of the soil and plant community patterns. This is particularly common in smaller watersheds, where coherence in spatial patterns of soil, geology and vegetation is pronounced because patterns of snow deposition, which control available water, and soil genesis are closely linked.

Twenty-five year (1984–2008) basin average water year (WY) precipitation and outflow from the RME watershed are 849 and 505 mm [34]. Over that period, 70% of precipitation fell as snow.

**Table 1**
Land cover in the Reynolds Mountain East watershed.

| Land cover | Symbol | Areal fraction | Comments |
|---|---|---|---|
| Aspen | As | 15.7% | Stands of large mature trees, mixed with willow and a few fir. Found either immediately downslope of snow drifts in upland areas, or in the riparian areas near the stream |
| Fir | F | 5.1% | Dominated by Douglas fir, found above and around the Aspen regions and just below several of the drift zones |
| Sage | S | 47.4% | Mountain big sagebrush either in dense stands with snowberry or sparse stands without snowberry |
| Ridge low sage | RLS | 12.9% | Little or no vegetation, sparsely covered by low sagebrush with mixed grasses and forbs |
| Drift Aspen | DAs | 11.2% | Dense clusters of distorted shrub-like trees that are covered by drifts during the snow season. Co-located with drift areas, though may not be completely covered during low snow years |
| Dry meadow | DM | 7.7% | Thin, rocky soils dominated by grasses and forbs |

Wind, topography and vegetation strongly affect the distribution of snow, which preferentially accumulates in drifts and wind-protected areas [36] that contribute nearly half its total surface water, though occupying less than one-third of the basin [43]. The wind-swept exposed ridges and low sagebrush areas generally accumulate less than 1 m of snow (~280 mm of snow water equivalent) during the winter. On the other hand, the drift area immediately upslope of the aspen and fir typically accumulates 6 m of snow (~1750 mm of snow water equivalent). Precipitation is strongly seasonal with dry summers and wet winters.

All distributed data and topological relations were mapped to the PIHM unstructured mesh and discretized linear river elements.

## 4. Data sets for forcing and validation

The RME catchment contains two primary climate stations [32,34]: the Reynolds Mountain climate station (elevation 2097 m), located on a broad shelf at the southwestern edge of the basin, and the Reynolds Mountain snow pillow site (elevation 2061 m), located within a forest opening (Fig. 1). Solar and thermal radiation, air temperature, humidity, wind speed and direction, and soil temperature are measured at both sites [34,44]. Site-measured values for all parameters are distributed over the watershed. Clear sky solar radiation, corrected for topography, is simulated over the elevation grid [45,46], and then corrected for clouds [34]. We correct for canopy attenuation by simulating the transfer of direct and diffuse radiation through various canopy types [47,48]. Snow albedo is adjusted for aging and effective snow grain size [26,49] and darkened because of litter deposition during melt [50] to account for the increasing exposure of dust and organic debris beneath the forest canopy [47]. Atmospheric longwave radiation based on surface temperature and humidity is calculated over the elevation grid [51] and scaled using measured values to account for the effect of clouds. Radiation under vegetation cover is further modified to account for the vegetation canopy [28,47]. Air temperatures are lapsed for elevations between the two measurement sites and distributed over the elevation grid. Measured relative humidity, assumed constant over the catchment because the differences between the two sites are generally less than instrument precision (over a larger basin, or one with a greater elevation range, this would not be the case), is converted to elevation-distributed dew point temperature using the distributed air temperatures [52]. Threshold dew point temperature of 0 °C during precipitation events is used to classify events as rain or snow [53]. Hourly spatial wind fields are generated using a model for topographic distribution of winds [36]. Precipitation, also measured at both sites, is corrected for wind-induced gauge undercatch [44,54] and then redistributed using information about topography and wind [35]. The redistribution process implicitly accounts for the loss due to sublimation during drifting. Measured near-surface soil temperatures were nearly constant below the snow, showing almost no difference between measurement sites, so this parameter is assumed to be spatially constant for all areas covered by snow. Over a larger basin, or one with a greater elevation range, this would not be the case. Validation data include snow water equivalent, water table elevation, soil moisture and streamflow. Water table elevation was continuously measured at groundwater wells (Fig. 1) using pressure transducers. Soil moisture was measured continuously at the meteorological site (SM3 in Fig. 1) using a dielectric method, and bi-weekly at two locations (SM1 and SM2 in Fig. 1) using neutron probes. Streamflow was measured at a V-notch weir [55].

## 5. Model application and calibration

Three linked simulations—Is+P, uncalTi+P and calTi+P—each simulated SWE, snowmelt and surface water input, overland flow and ponding, depth-averaged unsaturated soil moisture in the top 25 cm and the unsaturated zone below it, groundwater head at the centroid of each of the 3939 unstructured mesh elements, and stream stage in 49 stream sections (Fig. 1). The Is+P model also accounts for sublimation from accumulated snow. Interfacial fluxes such as infiltration and exfiltration, recharge to and from groundwater, evapotranspiration, and lateral groundwater exchange between discretized aquifer elements and between the aquifer and the stream are also calculated over the modeling domain at each time step. The model run for two water years starts on the first day of water year 2006 (2005 October 01) and ends on the last day of WY2007 (2007 September 30). The chosen simulation period ensures availability of transient validation data sets such as streamflow, groundwater elevation, snow water equivalent, and surface soil layer saturation, and allows validation at seasonal and interannual scales. The two years also present meteorologically diverse forcing conditions (Table 2). WY2006 was very wet, falling in the upper quartile of the historical record, while WY2007 was dry with total precipitation within the lower quartile. The precipitation distribution and the fraction of precipitation as rain for the two water years were also different. During the dry year, a larger percentage of precipitation fell during spring, mostly as rain when the snow was receding. The maximum SWE for 2007 was reached nearly five weeks earlier than in 2006.

## 6. Calibration of the temperature-index model

Isnobal requires no calibration. We calibrate the temperature-index model (calTi+P) by adjusting the temporally varying melt factor until an adequate match of the simulated to the observed SWE is obtained at the snow pillow site. Calibration of the hydrology model is performed independently of the melt inputs from snow model. The process involves nudging of hydrogeological parameters uniformly across the model domain, to match the magnitude and rate of the hydrograph decay during recession. Calibration is limited to the first year of the simulation. Two calibration periods are chosen: (1) a dry period with no appreciable antecedent recharge (10/10/2005 to 10/25/2005), and (2) a wet, cold period with peak streamflow response and negligible evapotranspiration (12/30/2005 to 01/30/2006). For hydrologic calibration, PIHM is first initialized by water table at the land surface and the model is allowed to relax with no precipitation input until streamflow approaches zero. The simulated relaxation hydrograph is compared with observed streamflow in the first calibration period. During this period, streamflow is dominated by

**Table 2**
Precipitation (mm) in water years 2006 and 2007.

| | WY2006 | WY2007 |
|---|---|---|
| Total precipitation | 1119 (32% above 25 year average) | 671 (22% below 25 year average) |
| Precipitation as snow | 877 (78% of total) | 391 (58% of total) |
| Date of maximum snow | 16 April | 07 March |
| Total precipitation before maximum snow | 977 (82% of total) | 489 (73% of total) |

baseflow, and antecedent recharge is negligible. To best approximate the below ground hydrogeologic function of the watershed, the PIHM calibration first ensures that both simulated groundwater level at the three locations and simulated streamflow hydrograph match the observed during baseflow. Hence the calibration process is first constrained by groundwater level at three locations and streamflow at the outlet. Next, the rate of relaxation in the simulated hydrograph is compared with observed during the second calibration period—a winter rain and snowmelt event when evapotranspiration is negligible. During the calibration procedure, van-Genuchten coefficients [56] and macro and matrix porosity and conductivity are adjusted by visually comparing the match between simulated and observed target metrics. Notably, the target metrics of the calibration strategy—the rate of hydrograph decay, magnitude of baseflow and spatial distribution of groundwater table depth—differ from validation metrics such as the match between simulated and observed streamflow time series and total water year water balance. The PIHM calibration process does not simply fit parameters to match validation objectives, but attempts to best match the behavior and response dynamics of the basin. More importantly, the PIHM calibration procedure is independent of the snowmelt forcing. This strategy avoids giving any preference to either of the snow models in determining performance of integrated hydrologic simulations. It also ensures that comparisons of the integrated snow and hydrology models do not depend on a calibration strategy that varies with the snowmelt formulation used. The same distributions of calibrated hydrogeologic parameters are used in all three model simulations.

## 7. Results

The results focus on comparison of distributed SWE as predicted by temperature-index and energy-balance snow models, and its consequent role on watershed response.

### 7.1. SWE and snow cover

SWE predictions are first compared to observed data at the snow pillow site (Fig. 2(a)). The Is+P and calTi+P models simulate SWE at the snow pillow site reasonably well for both years (Table 3). *NSE* for calTi+P simulated SWE for the two years is as large as 0.98 and 0.96, demonstrating that the calibration of melt factors adequately captures snow accumulation and melt at the snow pillow site. In contrast, uncalibrated temperature-index (uncalTi+P) simulation, replicates the snow accumulation at the observation site reasonably well, but under-predicts melt rate during late spring and early summer. Hence, *NSE* for uncalTi+P simulated SWE for the two years is only 0.78 and 0.77.

Even though the predicted SWE from Is+P and calTi+P models are both good at the observation location, the spatio-temporal distributions of SWE are markedly different. Fig. 3 shows maps of SWE for December 14, March 4, April 28 and May 14 for WY2007. December 14 corresponds to conditions just after a rain-on-snow event; March 4 is just before the start of spring melt when the snow cover is near its maximum; spring streamflow is at its peak on April 28, and May 14 represents the conditions just after melt-out of accumulated snow at the snow pillow site. Although the three models are forced by the same heterogeneous precipitation, for the four days shown in Fig. 3, watershed averaged SWE predicted by the uncalTi+P and calTi+P models are consistently larger than that predicted by Is+P (Fig. 3). The calTi+P and uncalTi+P SWE volumes are twice that predicted by Is+P on December 14, and 134% on March 4. By April 28 calTi+P SWE is still double that of Is+P and uncalTi+P SWE is four times greater. By May 14, the snow is nearly gone in both the calTi+P and Is+P models, though the uncalTi+P model still retains more than 100 mm SWE. Additionally the snow covered area (SCA) predicted by calTi+P model is higher than by Is+P model for all but the second date (March 4), when all models show 100% SCA. For December 14, Is+P shows SCA at about 94%, while both temperature-index models show 100%. For April 28, Is+P shows about 31% SCA, while calTi+P shows 86%, and uncalTi+P 99%. By May 14, with the exception of a few drifts, the snow has melted in Is+P and calTi+P, but the uncalTi+P model shows more than 84% SCA.

### 7.2. Soil moisture and groundwater

The Is+P, uncalTi+P, and calTi+P models capture the observed soil moisture fluctuations, at the soil moisture measurement sites (Fig. 1), to varying degrees of success (Fig. 2(b)–(d)). At SM3, the only site with hourly data, all models capture the soil moisture with about the same coefficient of determination (*CD*) in the calibration year (WY 06), but the Is+P model captures the dry year more accurately (Table 3). Is+P model also performs better at sites SM1 and SM2, however the performances in general are relatively worse than at SM3. Notably, simulated soil moisture at SM2 during dry year (Fig. 2(c)) completely misses wet conditions in early winter. This is because surface soil layer at the exposed site freezes, as corroborated by the soil temperature data, which results in limited soil water drainage and hence a very high soil moisture readings due to ponding. PIHM, however, does not simulate the dynamic change in soil temperature and its effects on hydraulic conductivity. In contrast, because of a deeper early season snow cover, both the soil temperature and moisture data indicate that soil freezing did not occur at sites SM1 or SM3. The differences in spatial variations of soil moisture as predicted by the three model configurations are shown in Fig. 5. On December 14, just after rain-on-snow event, the Is+P model shows substantially greater saturation (0.47) than either Ti+P simulation (0.34 and 0.35, Fig. 5). On Mar. 4 all three models show similar soil saturation, with some of the early season soil moisture still evident in the Is+P simulation. On April 28, the day streamflow peaks, the average soil saturations between the model simulations differ starkly, with high soil saturation (0.60) for the calTi+P simulation, while saturation simulated by Is+P and uncalTi+P are similar (0.51 and 0.49). By May 14, when the snow pillow site is again snow free, the soil moisture is depleted in both Is+P and calTi+P simulations (Fig. 5), while the uncalTi+P still shows higher soil saturation.

Comparisons of simulated groundwater head are performed at three well locations in the watershed (Fig. 2(e)–(g)). It is to be noted that observed groundwater responses at the three wells are very distinct. At the first two sites, groundwater depth varied as much as 7.5 m in a matter of three hours. The water table variation at GW3 (Fig. 2(g)) is relatively muted. Simulated GW results from the Is+P and calTi+P models are similar at respective sites, as they capture the rapid short-term and slower seasonal variations. The results do not highlight a significant improvement in prediction by any one of the model simulations over other.

### 7.3. Evaporative fluxes

The Is+P model simulates three evaporative components: Sublimation\Condensation, Transpiration and Ground evaporation. Ti models (calTi+P and uncalTi+P) simulate only two evaporative components, as they do not account for Sublimation or Condensation.

Sublimation losses simulated by Is+P model are largest over exposed land covers and during periods with high wind speeds. A map of modeled sublimation and condensation (Fig. 6) shows higher values near the southwestern edge of the watershed where snow is more exposed to prevailing winds. Positive values in the

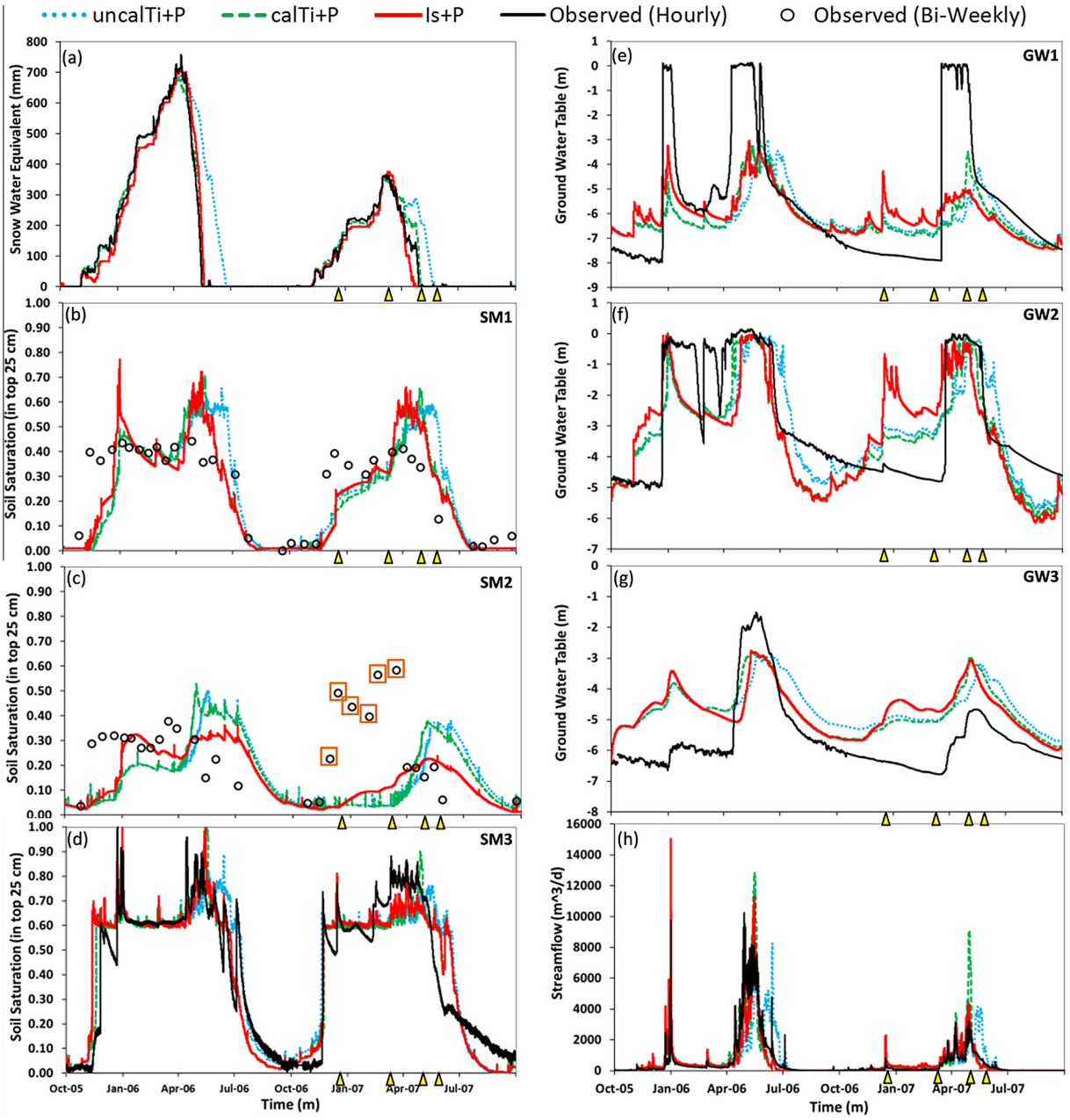


**Fig. 2.** Observed and modeled (a) snow water equivalent, (b)–(d) surface soil saturation, (d)–(f) water table depth from surface at GW1, GW2 and GW3 wells, and (g) streamflow, in RME watershed for two water years beginning October 01, 2005. Pointers on the *x*-axis identify the days of interest (December 14, March 4, April 28 and May 14). Bi-weekly soil moisture observations with rectangle around them indicate frozen soil conditions.

**Table 3**
Comparison metrics between observed and simulated states of water years 2006 and 2007. *CD* = Coefficient of Determination; *NSE* = Nash Sutcliffe Efficiency. SM1, SM2 and SM3 represent statistics for soil saturation in top layer at the three soil moisture observation sites.

| | | SWE | | Streamflow | | SM1 | | SM2 | | SM3 | |
|---|---|---|---|---|---|---|---|---|---|---|---|
| | | WY'06 | WY'07 | WY'06 | WY'06 | WY'06 | WY'07 | WY'07 | WY'07 | WY'06 | WY'07 |
| CD | Is+P | 0.99 | 0.98 | 0.87 | 0.91 | 0.72 | 0.80 | 0.30 | 0.19 | 0.91 | 0.93 |
| | uncalTi+P | 0.91 | 0.90 | 0.66 | 0.70 | 0.65 | 0.73 | −0.11 | −0.26 | 0.92 | 0.89 |
| | calTi+P | 1.0 | 0.98 | 0.89 | 0.84 | 0.65 | 0.74 | 0.00 | −0.19 | 0.93 | 0.91 |
| *NSE* | Is+P | 0.98 | 0.95 | 0.73 | 0.60 | −0.00 | 0.54 | −0.46 | −0.15 | 0.81 | 0.85 |
| | uncalTi+P | 0.78 | 0.77 | 0.42 | −0.22 | −0.19 | 0.40 | −1.38 | −0.87 | 0.84 | 0.78 |
| | calTi+P | 0.99 | 0.96 | 0.73 | −0.82 | −0.35 | 0.41 | −1.22 | −0.72 | 0.86 | 0.82 |

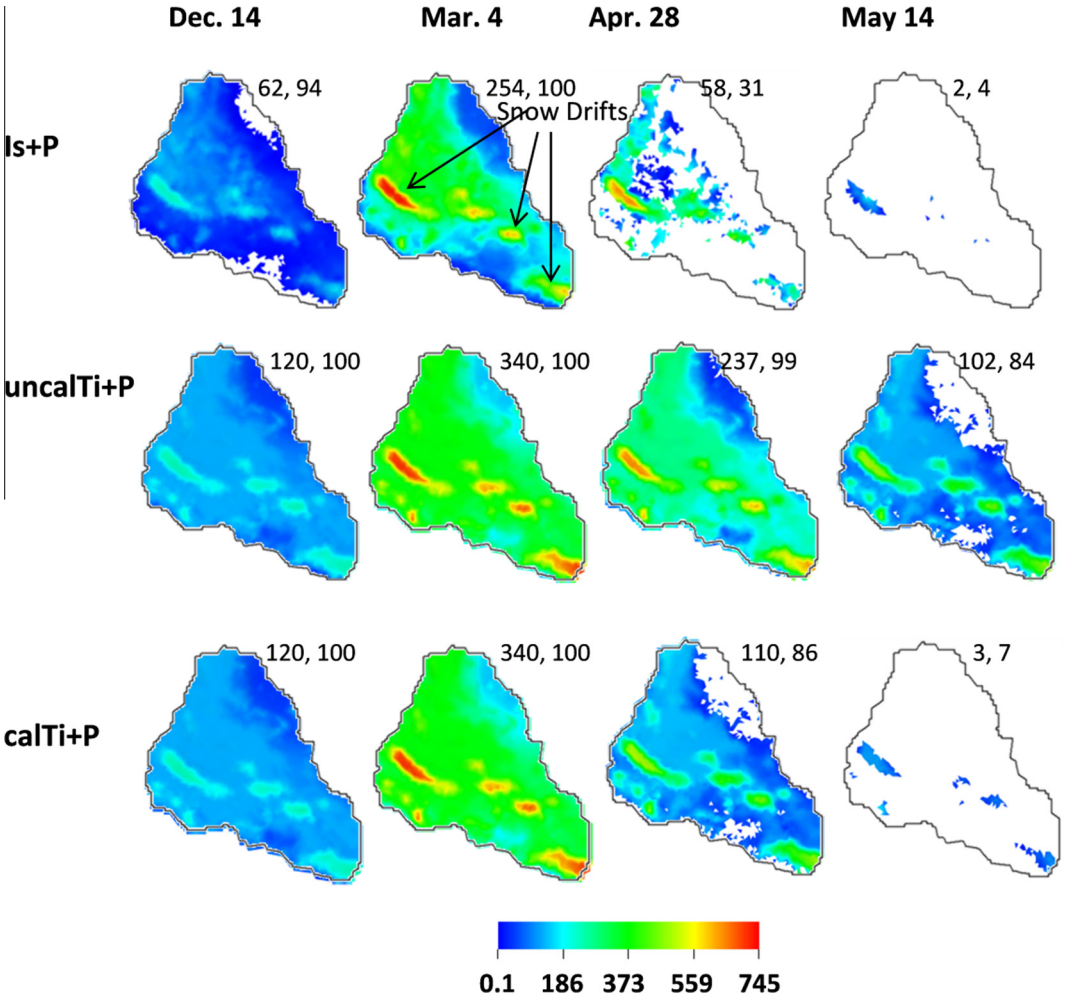


**Fig. 3.** Spatial and temporal variation of snow water equivalent (mm) for WY2007 as simulated by Is+P, uncalTi+P and calTi+P models. Pair of numbers (separated by comma) on the right top corner of each plate represents the average SWE for the day and percent snow cover area respectively. December 14 ≡ Rain-on-snow event, March 4 ≡ Maximum SWE at snow pillow, April 28 ≡ Peak streamflow response, May 14 ≡ Melt-out date at snow pillow

map correspond to condensation while negative values denote sublimation. While the northeastern edge of the watershed is also exposed, strong winds scour the snow, resulting in a smaller net sublimation loss. The Is+P model simulates average sublimation losses of 34 and 35 mm during the dry and wet years. The 2 years experienced condensation of 18 and 25 mm, mostly in periods of higher humidity such as during rain events. As a result, net sublimation simulated by Is+P is 17 and 10 mm during dry and wet year.

Simulated transpiration by the three model configurations show a distinct heterogeneous pattern (Figure ure6) that mirrors distribution of vegetation leaf area indices in the watershed. Mean transpiration losses, as simulated by Is+P model, for the land cover types *As*, *F*, *S*, *RLS*, *DAs* and *DM* are 366, 538, 52, 5, 203 and 96 mm. Transpiration losses are largest from Fir and least from *RLS*. Notably, the simulated magnitude of transpiration for WY2007 in Aspen is 364 mm while the measured transpiration at the flux tower over Aspen calculated from eddy-covariance data [57] was 314 mm. Additional eddy-covariance measurements from the exposed site were available, but were not used because they include fluxes from outside the watershed. In relation to transpiration simulated by Is+P, WY rates simulated by calTi+P are smaller in Aspen (*As*) and Fir (*F*) and larger or equal to in all other land covers (Table 4). In spite of the expressed differences in transpiration rates in different land covers, watershed averaged WY transpiration values simulated by Is+P and calTi+P models are almost the same, 146 and 141 mm. The transpiration simulated by the uncalTi+P model, however, is much larger and is equal to 169 mm.

The simulated evaporation losses by Is+P and calTi+P models are also only marginally different (Table 4). The evaporation simulated by the uncalTi+P model, however, is much smaller than other two simulations.

### 7.4. Streamflow

Although the SWE prediction at the snow pillow site for Is+P and calTi+P simulations are adequate for both water years, the streamflow prediction is much worse for calTi+P simulations, especially in dry validation WY 2007 (Fig. 2(h) and Table 3). The coefficient of discharge (*CD*) and Nash–Sutcliffe efficiency (*NSE*) of simulated streamflow using Is+P model are 0.87 and 0.73 (Fig. 2(h)) for the two-year simulation. The corresponding values for calTi+P and uncalTi+P simulated streamflow are 0.86 and 0.63, and 0.66 and 0.40 respectively. The performance of uncalTi+P model is even worse, as predicted streamflow peak is delayed by nearly a month in both years (Fig. 2(h)). In regards to the estimate of average water year streamflow, streamflow simulated by the Is+P model is 551 mm (62% of total precipitation), 20 mm more

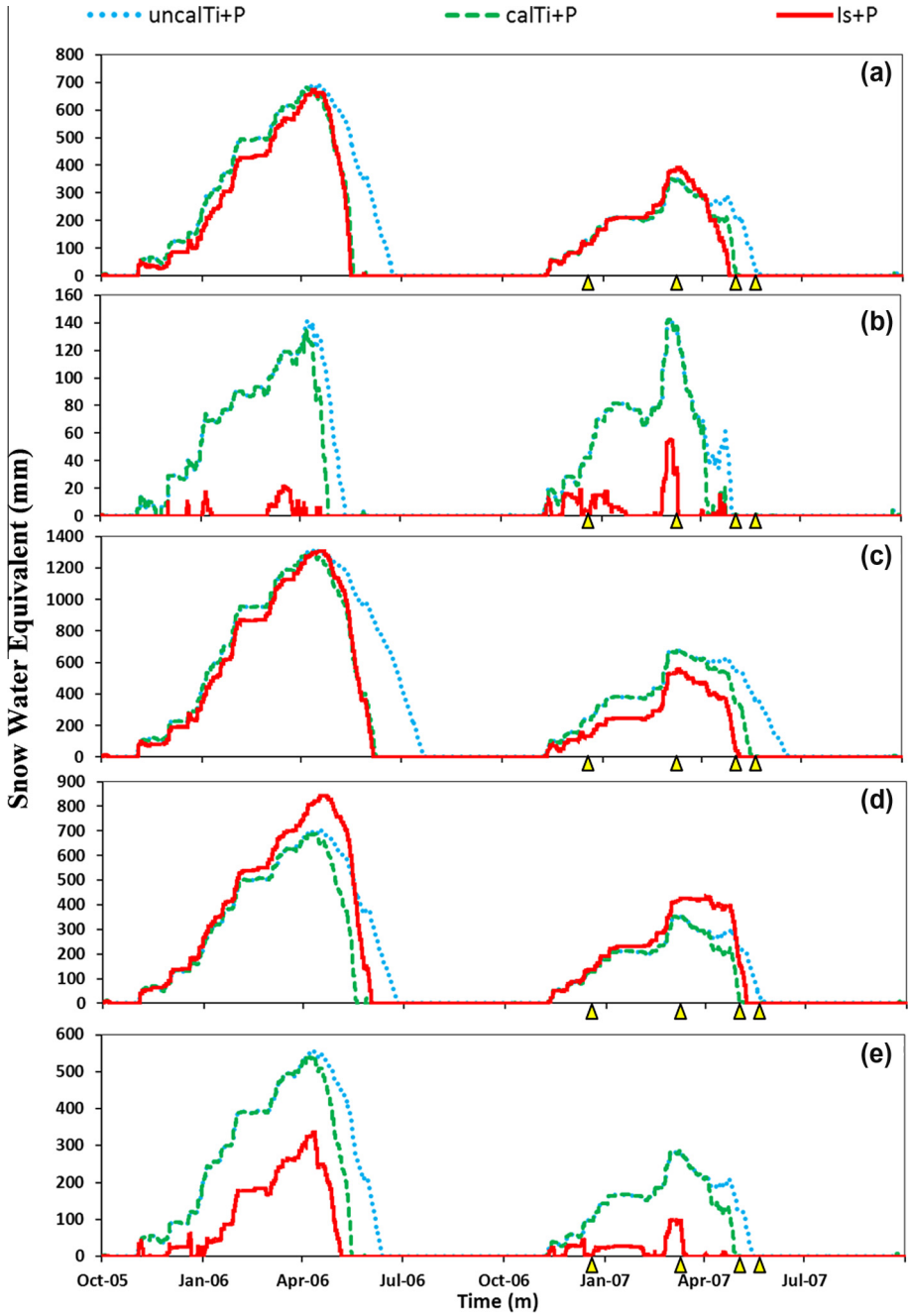


**Fig. 4.** Temporal variation of snow water equivalent (mm) for WY2007 as simulated by Is+P, uncalTi+P and calTi+P models at five locations within the watershed. The locations (a) to (e) are identified in Fig. 1. Pointers on the *x*-axis identify the days of interest (December 14, March 4, April 28 and May 14).

than the observed streamflow. Comparatively, the uncalTi+P and calTi+P models simulated a much larger than observed streamflow of 564 and 572 mm, in part due to a smaller net evaporative flux simulated by temperature index models (Tables 4 and 5).

### 7.5. Interannual water balances

Because the three model configurations predict different snow distributions, extents, duration, and melt rates, the net water balance simulated by the three model configurations also varies. Over the 2-year simulation period, average output from the watershed using the Is+P model amounted to 898 mm, only 3 mm larger than the precipitation. Comparatively, uncalTi+P and calTi+P models yielded an average output of 902 and 905 mm. The results show that over the simulation period, the watershed accumulated net storage in Is+P simulation but lost net storage in uncalTi+P and calTi+P simulations (Table 5). Observations at three groundwater wells corroborate this behavior. The net observed groundwater elevation at the observation sites increased by 439.5 mm during wet year, and decreased only by −372.5 mm during the dry year. The same trend is exhibited in Is+P simulations. However, calTi+P simulations showed a net decrease in groundwater storage (Table 5) for both the years.

## 8. Discussions

The results clearly highlight that adequately calibrated temperature index model simulations (calTi+P) show considerable

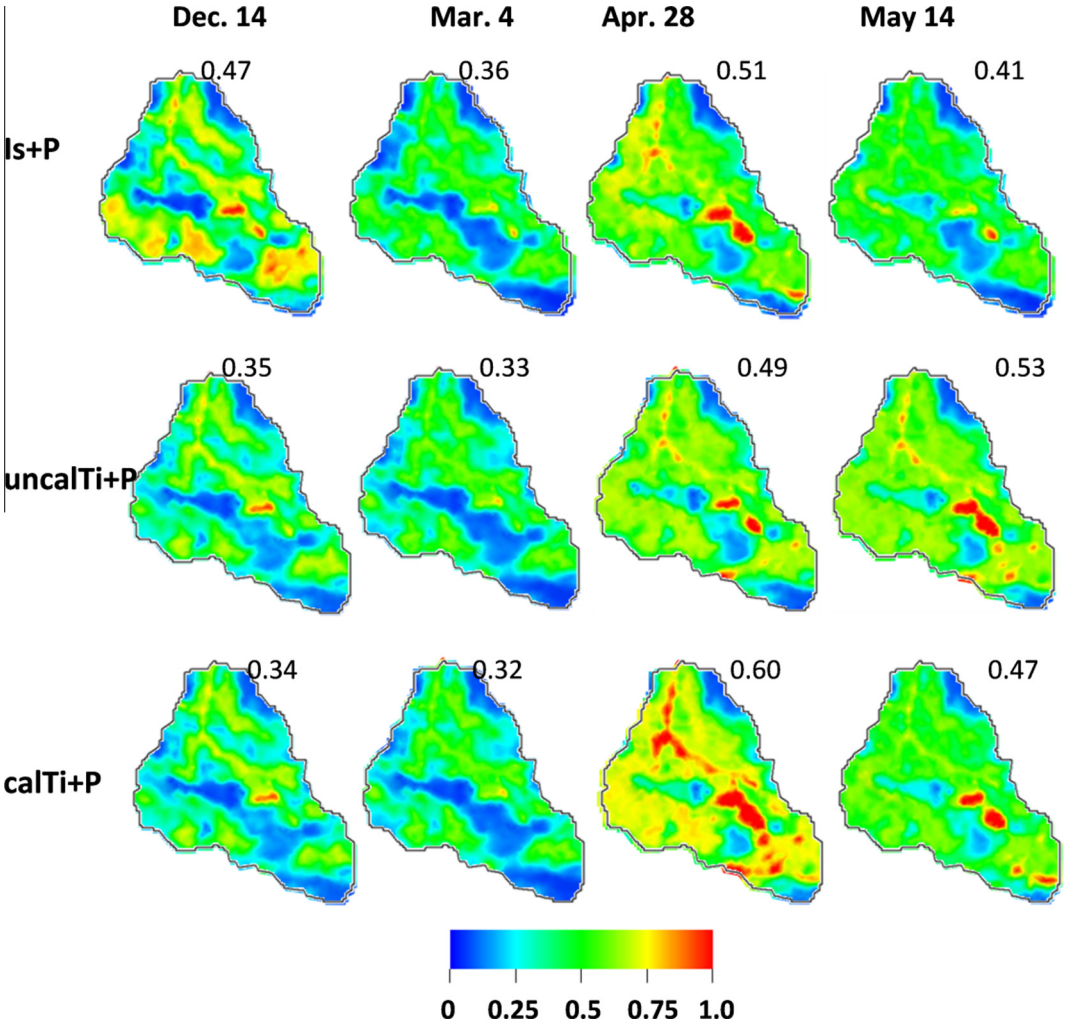


**Fig. 5.** Spatial and temporal variation of soil moisture (in top 25 cm) saturation for WY2007, as simulated by Is+P, uncalTi+P and calTi+P models. Numbers on the right top corner of each plate represents the spatial average of the quantity. December 14 ≡ Rain-on-snow event, March 4 ≡ Maximum SWE at snow pillow, April 28 ≡ Peak streamflow response, May 14 ≡ Melt-out date at snow pillow

differences from energy-based snow simulations (Is+P) in distributed estimates of hydrologic states. This is primarily because in the Isnobal simulation, topography and vegetation modulate solar radiation, wind and air temperature, which results in heterogeneous melt rate throughout the watershed. In contrast, the temperature-index models use a uniform melt factor over the whole watershed and only account for distributed temperature variation. The calibrated melt factor in calTi+P model is derived at the snow pillow site, which is located in an Aspen grove. The site is somewhat sheltered from radiation and wind. Therefore, use of a spatially uniform temperature-index melt factor, calibrated to fit conditions at the snow pillow site, over the whole watershed leads to under-prediction of the melt rate in the more exposed *S*, *RLS* and *DA* land cover areas. As a result, SWE in these exposed land cover areas are over-predicted by calTi+P model (Fig. 4(b), (c) and (e)). For the same reason, melt rate in sheltered areas, such as in *F* where shading is much more intense and wind speeds are even lower than at the snow pillow site, is over-predicted. This results in under-prediction of SWE in *F* (Fig. 4(d)). Since the areal extent of exposed areas (*S* and *RLS*) is large (nearly 60% of the watershed), the net increase in watershed averaged SWE due to lower melt rate in exposed areas is greater than the net decrease due to higher melt rate in sheltered areas from the calTi+P model. Hence, calTi+P fails to capture early season melt in the exposed areas and predicts greater watershed-wide volumes of SWE over the catchment on the four dates shown, compared to Is+P (Fig. 3).

The reported disparities in melt rates between the three model configurations in both exposed and sheltered regions of the watershed (Fig. 4), also explains the emergent differences in consequent hydrologic response. Case in point are the differences in spatial and temporal distribution of soil saturation. On December 14, right after the rain-on-snow event, the Is+P model shows substantially greater saturation (0.47, Fig. 5) than either Ti+P simulation (0.34 and 0.35, Fig. 5), as it accounts for extensive melt due to transfer of latent and sensible heat flux toward the snow surface. On Mar. 4 all three models show similar soil saturation, with some of the early season soil moisture still evident in the Is+P simulation. By April 28, the average soil saturations between the model simulations differ starkly, with high soil saturation (0.60) for the calTi+P simulation, while saturation simulated by Is+P and uncalTi+P are similar (0.51 and 0.49). This is primarily because calTi+P simulation overestimates SWE in exposed areas of the watershed resulting in delayed melt. Additionally the overestimated snow, melts everywhere at a similar rate resulting in excess melt and hence a higher average soil saturation. By May 14 the snow is depleted in both Is+P and calTi+P simulations (Fig. 4), while snow cover in the uncalTi+P simulation is still large and generates significant melt recharge resulting in higher soil saturation.

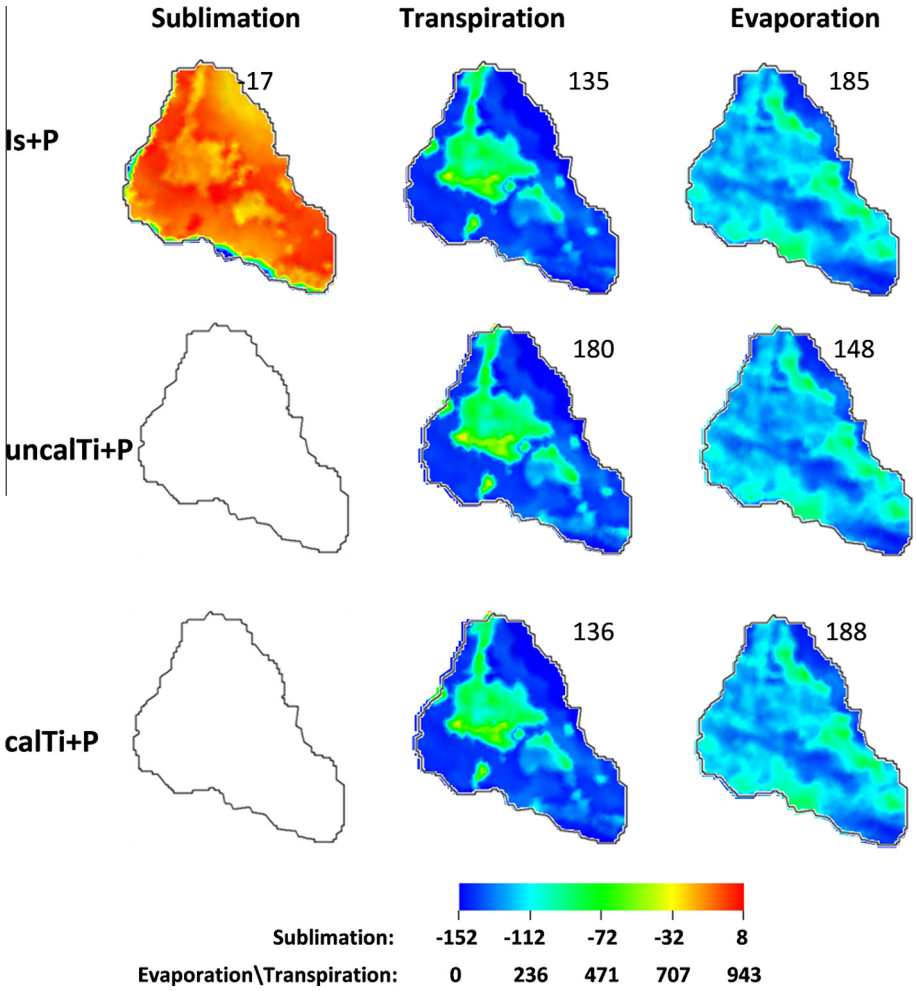


**Fig. 6.** Spatial variation of sublimation, transpiration and evaporation (in mm) as simulated by Is+P, uncalTi+P and calTi+P models for WY2007. Numbers on the right top corner of each plate represent the annual magnitude of the variable.

**Table 4**
Annual water losses (mm) due to Evaporation, Transpiration and Sublimation by land cover type for the two year simulation period.

| | | Transpiration Annual Average | | | Evaporation Annual Average | | | Sublimation Annual Average | | |
|---|---|---|---|---|---|---|---|---|---|---|
| | | Is+P | uncalTi+P | calTi+P | Is+P | uncalTi+P | calTi+P | Is+P | uncalTi+P | calTi+P |
| Aspen | As | 366 | 385 | 351 | 195 | 165 | 192 | 14 | – | – |
| Fir | F | 538 | 588 | 520 | 140 | 125 | 143 | 13 | – | – |
| Sage | S | 52 | 58 | 53 | 228 | 217 | 229 | 12 | – | – |
| Ridge Low Sage | RLS | 5 | 5 | 5 | 73 | 70 | 72 | 18 | – | – |
| Drift Aspen | DAs | 203 | 281 | 210 | 136 | 125 | 143 | 14 | – | – |
| Dry Meadow | DM | 96 | 104 | 99 | 283 | 266 | 285 | 13 | – | – |

**Table 5**
Water balances (mm) of water years 2006 and 2007. Percentages denote the magnitude of variable with respect to total precipitation.

| | | | Is+P | | uncalTi+P | | calTi+P | |
|---|---|---|---|---|---|---|---|---|
| | | | WY06 | WY07 | WY06 | WY07 | WY06 | WY07 |
| Input | | Total precipitation | 1119 | 671 | 1119 | 671 | 1119 | 671 |
| Output | | Stream discharge | 752 (67%) | 350 (52%) | 758 (68%) | 371 (55%) | 781 (70%) | 364 (54%) |
| | | Evaporation | 199 (18%) | 185 (28%) | 169 (15%) | 148 (22%) | 199 (18%) | 188 (28%) |
| | Total ET | Transpiration | 146 (13%) | 135 (20%) | 177 (16%) | 180 (27%) | 141 (13%) | 136 (21%) |
| | | Net Sublimation | 10 (1%) | 17 (3%) | – | – | – | – |
| Net storage change | | Input–Output | +12 | −15 | +15 | −28 | −2 | −17 |

Differences in snow extent and duration, as calculated by the three model configurations, also influences evapotranspiration by affecting the spatio-temporal distribution and amount of sublimation losses, melt recharge to the soil, and shielding of soil from the atmosphere. For example, transpiration rates simulated by Is+P in sheltered (*As* and *F*) land covers are larger than that simulated by

calTi+P model (Table 4), because of interplay between the availability of moisture in the root zone and meteorological conditions that support transpiration. In the calTi+P model, estimated melt rate is larger for sheltered land covers, which means that more moisture is delivered to the root zone early in the melt season when net radiation is less. As a result, predicted transpiration rates in the early melt season are larger for calTi+P simulations. But this translates to depleted moisture availability during the period when incoming solar radiation is larger and temperatures are warmer. On the other hand, while the melt rate predicted by Is+P model for *As* and *F* is smaller, it is sustained for a longer period. Delayed melt coincides with a period of larger potential transpiration rates causing predicted transpiration rates to be larger late in the melt season. Late season increases offset the decrease in transpiration during early melt. This results in a higher seasonal transpiration predicted by the Is+P model. For similar reasons, annual transpiration rates simulated by calTi+P in other land cover types (*S*, *RLS*, *DAs* and *DM*) are equal to or greater than rates simulated by the Is+P model, as melt rates predicted by the Is+P model in these land cover types are larger. This also results in a larger predicted WY transpiration by uncalTi+P, where delayed snowmelt leads to increased water availability later in the summer when potential transpiration is the greatest.

Interplay between melt and duration of snow cover also influences the amount of simulated evaporation. Water loss through evaporation proceeds at the potential evaporation rate as long as the ground is snow-free and surface moisture is sufficient. The snow effectively shields the mass exchange between the soil and atmosphere, limiting evaporation. So on the one hand, greater snow extent reduces soil evaporation, but on the other such conditions contribute to an extended melt period and melt recharge well into the growing season, increasing soil moisture during periods with greater potential evaporation. The variation in evaporation with snow extent and timing of melt-out within a land cover category are controlled by the competition between increased evaporation because of extended soil moisture and reduced evaporation because of extended snow duration, which shields the soil from evaporative demand. Incidentally, this results in only marginal difference in total WY evaporation rated between Is+P and calTi+P simulation (Table 4). The interplay of competition on evaporation is however strongly expressed in wet and dry years. Soil evaporation simulated by Is+P model in the wet year is only 13 mm higher than in dry year, even though the precipitation was 448 mm higher (Table 5). A larger evaporation to precipitation ratio for the dry year is observed also in the uncalTi+P and calTi+P models.

Because of overestimation of SWE in exposed areas of the watershed, combined with the near uniform melt rate across the watershed and only marginal change in evapotraspirative losses, simulated streamflow peak in calTi+P simulations overestimates the observed, especially in the dry validation year.

## 9. Conclusions

This study evaluates the differences in predicted hydrologic states from integrated hydrologic models that use either energy-balance or temperature-index snow models to simulate the ablation of the snowpack. Comparisons between alternate model configurations explore, compare and contrast the spatio-temporal distribution of snow accumulation and melt, and its consequent impact on surface and subsurface hydrologic states and fluxes across multiple land cover types.

Results show that even though the predicted SWE from Is+P and calTi+P models were reasonably good at the observation location, snow accumulation and melt calculations in different land covers are sensitive to the choice of the modeling approach. calTi+P under-predicts melt in more exposed areas and over-predicts in sheltered areas where shading is much more intense and wind speeds are low. This indicates that calibrated melt factors obtained from calTi+P model at the snow pillow site, even in smaller watersheds, do not realistically apply everywhere in the watershed, and should be derived for multiple locations with different snow deposition, wind and radiation exposures for appropriate quantification of watershed averaged melt. The energy-balance model requires no such distributed calibration. In contrast, uncalTi+P under-predicts melt during late spring and early summer. Since these periods are critical for recharge, water storage and runoff, temperature-index models that are not sufficiently calibrated should be used with caution.

Additional comparisons illustrate the consequent hydrologic influence of differences in snow accumulation, melt rates and duration between Is+P, calTi+P and uncalTi+P models. Influence of model strategy on streamflow prediction is significant. The peak streamflow simulated by the calTi+P model is much larger than observed because of overestimation of SWE in exposed areas of the watershed. It is to be highlighted here that if the aerial fraction of sheltered areas in a watershed had been much larger, peak streamflow at the watershed outlet from the calTi+P model would be expected to under-predict (instead of over-predict) the observed, even when SWE prediction at the observation site was accurate. The temperature index approach, with melt factors calibrated in a wet year, also simulates a much different distribution, timing and magnitude of soil moisture in dry year in relation to Is+P model. At an event scale, because the uncalTi+P and calTi+P models do not account for the large latent and sensible heat fluxes toward the snow surface during rain-on-snow, they under-predict soil saturation after rain-on-snow at the exposed sites. Additionally, because of over-prediction of SWE in exposed areas and use of a uniform melt factor within the watershed, the temperature index models simulate a delayed soil moisture peak. The differences in evapotranspirative fluxes between different model strategies show a consistent trend in different land covers, based on how sheltered or exposed the land cover is with respect of snow pillow site. In comparison to the Is+P simulation, calTi+P simulates less transpiration in sheltered land covers (*As* and *F*) and more transpiration in the more exposed land cover types (*S*, *RLS, DAs* and *DM*). Incidentally, the catchment-integrated ground evaporation and transpiration fluxes predicted by Is+P and calTi+P models are similar. However, depending on the duration of snow cover, the timing of melt recharge in relation to net radiation, and the aerial fraction of sheltered vs. exposed areas in the watershed, evapotranspirative fluxes between Is+P and calTi+P simulations can be significantly different. Notably, temperature-index models (calTi+P and uncalTi+P) do not account for sublimation from accumulated snow. While not so important to the mass balance of the RME basin where sublimation rarely exceeds 5% of precipitation [58], this would be critical in colder regions with less precipitation where sublimation can exceed 25% of precipitation [59].

In conclusion, snow model configurations have strong bearing on distributed estimates of hydrologic states, but the differences are also strongly influenced by meteorological setting and landcover patterns in the watershed. The experiment shows the value of using an EB snow model over TI snow models, demonstrates the value of considering spatially distributed controls for better hydrologic predictions, and underscores the importance of high resolution spatial and temporal data sets.

## Acknowledgements

The data and analysis presented in this paper were funded in part by Duke University startup grant, NASA NNX11AK35A, NSF CBET-0838607, NSF-CBET (0854553), USDA-ARS CRIS Snow and

Hydrologic Processes in the Intermountain West (5362-13610-008-00D), USDA-NRCS Water and Climate Center-Portland, Oregon (5362-13610-008-03R), USDA-ARS Headquarters Postdoctoral Research Associate Program-Class of 2009 (0101-88888-016-00D), USDA-NRCS Conservation Effects Assessment Project (5352-13610-009-14R), USDA-ARS CRIS Preserving water quality and availability for agriculture in the Lower Mississippi River Basin (7408-13000-024-00D). Any reference to specific equipment types or manufacturers is for information purposes and does not represent a product endorsement or recommendation. USDA is an equal opportunity provider and employer.

## References

[1] Winstral A, Elder K, Davis RE. Spatial snow modeling of wind-redistributed snow using terrain-based parameters. J Hydrometeorol 2002;3:524–38. http://dx.doi.org/10.1175/1525-7541(2002)003<0524. SSMOWR>2.0.CO;2.
[2] Williams CJ. JP McNamara, DG Chandler. Controls on the spatial and temporal variation of soil moisture in a mountainous landscape: the signatures of snow and complex terrain. Hydrol Earth Syst Sci 2009;13:1325–36. http://dx.doi.org/10.5194/hess-13-1325-2009.
[3] Dozier J. Mountain hydrology, snow color, and the fourth paradigm. Eos Trans AGU 2011;92:373–4. http://dx.doi.org/10.1029/2011EO430001.
[4] Lundquist JD. MD Dettinger. How snowpack heterogeneity affects diurnal streamflow timing. Water Resour Res 2005;41:W05007. http://dx.doi.org/10.1029/2004WR003649.
[5] Elder K, Dozier J, Michaelsen J. Snow accumulation and distribution in an alpine watershed. Water Resour Res 1991;27:1541–52. http://dx.doi.org/10.1029/91WR00506.
[6] Marks D, Dozier J. Climate and energy exchange at the snow surface in the alpine region of the Sierra Nevada, 2, Snow cover energy balance. Water Resour Res 1992;28:3043–54. http://dx.doi.org/10.1029/92WR01483.
[7] Dozier J, Painter TH. Multispectral and hyperspectral remote sensing of alpine snow properties. Ann Rev Earth Planet Sci 2004;32:465–94. http://dx.doi.org/10.1146/annurev.earth.32.101802.120404.
[8] Link TE, Marks D. Distributed simulation of snowcover mass- and energy-balance in the boreal forest. Hydrol Proc 1999;13:2439–52. http://dx.doi.org/10.1002/(SICI)99-85(199910)13:14/15<2439::AID-HYP866>3.0.CO;2-1.
[9] Harding R, Pomeroy J. The energy balance of the winter boreal landscape. J Climate 1996;9:2778–87. http://dx.doi.org/10.1175/1520-0442(1996)009<2778:TEBOTW>2.0.CO;2.
[10] Hardy J, Melloh R, Robinson P, Jordan R. Incorporating effects of forest litter in a snow process model. Hydrol Proc 2000;14:3227–37. http://dx.doi.org/10.1002/1099-1085(20001230)14:18<3227::AID-HYP198>3.0.CO;2-4.
[11] Cazorzi F, Dalla Fontana G. Snowmelt modelling by combining air temperature and a distributed radiation index. J Hydrol 1996;181:169–87. http://dx.doi.org/10.1016/0022-1694(95)02913-3.
[12] Hock R. A distributed temperature-index ice- and snowmelt model including potential direct solar radiation. J Glaciol 1999;45:101–11.
[13] Daly SF, Davis R, Ochs E, Pangburn T. An approach to spatially distributed snow modelling of the Sacramento and San Joaquin basins, California. Hydrol Proc 2001;14:3257–71. http://dx.doi.org/10.1002/1099-1085(20001230)14:18<3257::AID-HYP199>3.0.CO;2-Z.
[14] Quick MC. A pipes. UBC watershed model. Hydrol Sci Bull 1977;22:153–61. http://dx.doi.org/10.1080/02626667709491701.
[15] Martinec J, Rango A. Parameter values for snowmelt runoff modelling. J Hydrol 1986;84:197–219. http://dx.doi.org/10.1016/0022-1694(86)90123-x.
[16] Anderson EA. Snow accumulation and ablation model. 2006. p. 61.
[17] Jordan R. A one-dimensional temperature model for a snow cover: technical documentation for SNTHERM.89. US Army Cold Regions Research and Engineering Laboratory: Hanover; NH, 1991. p. 49.
[18] Liston GE, Elder K. A distributed snow-evolution modeling system (SnowModel). J Hydrometeorol 2006;7:1259–76. http://dx.doi.org/10.1175/JHM548.1.
[19] Flerchinger GN, Saxton KE. Simultaneous heat and water model of a freezing snow-residue-soil system, I. Theory and development. Trans Am Soc Civil Eng 1989;32:565–71.
[20] Tarboton DG, Luce CH. Utah energy balance snow accumulation and melt model (UEB) computer model technical description and users guide. Utah Water Research Laboratory: Logan, UT; 1996.
[21] Marks D, Domingo J, Susong D, Link T, Garen D. A spatially distributed energy balance snowmelt model for application in mountain basins. Hydrol Proc 1999;13:1935–59. http://dx.doi.org/10.1002/(SICI)1099-1085(199909)13:12/13<1935::AID-HYP868>3.0.CO;2-C.
[22] Lehning M, Bartelt P, Brown B, Fierz C. A physical SNOWPACK model for the Swiss avalanche warning, Part III: Meteorological forcing, thin layer formation and evaluation. Cold Regions Sci Technol 2002;35:169–84. http://dx.doi.org/10.1016/S0165-232X(02)00072-1.
[23] Fierz C, Riber P, Adams EE, Curran AR, Föhn PMB, Lehning M, et al. Evaluation of snow-surface energy balance models in alpine terrain. J Hydrol 2003;282:76–94. http://dx.doi.org/10.1016/s0022-1694(03)00255-5.
[24] Kumar M. Toward a hydrologic modeling system. The Pennsylvania State University. ProQuest Dissertations and Theses, 274. http://search.proquest.com/docview/3049843472accountid=10598.
[25] DeBeer CM, Pomeroy JW. Simulation of the snowmelt runoff contributing area in a small alpine basin. Hydrol Earth Syst Sci 2010;14:1205–19. http://dx.doi.org/10.5194/hess-14-1205-2010.
[26] Marks D, Kimball J, Tingey D, Link T. The sensitivity of snowmelt processes to climate conditions and forest cover during rain-on-snow: a case study of the Pacific Northwest flood. Hydrol Proc 1998;12:1569–87. http://dx.doi.org/10.1002/(sici)1099-1085(199808/09)12:10/11<1569::aid-hyp682>3.0.co;2-l.
[27] Garen DC, Marks D. Spatially distributed energy balance snowmelt modelling in a mountainous river basin: estimation of meteorological inputs and verification of model results. J Hydrol 2005;315:126–53. http://dx.doi.org/10.1016/j.jhydrol.2005.03.026.
[28] Susong D, Marks D, Garen D. Methods for developing time-series climate surfaces to drive topographically distributed energy- and water-balance models. Hydrol Proc 1999;13:2003–21. http://dx.doi.org/10.1002/(sici)1099-1085(199909)13:12/13<2003::aid-hyp884>3.0.co;2-k.
[29] Knox SH, Carey SK, Humphreys ER. Snow surface energy exchanges and snowmelt in a shrub-covered bog in Eastern Ontario, Canada. Hydrol Proc 2012;26:1876–90. http://dx.doi.org/10.1002/hyp.9289.
[30] Marks D, Dozier J, Davis RE. Climate and energy exchange at the snow surface in the alpine region of the Sierra Nevada, 1, meteorological measurements and monitoring. Water Resour Res 1992;28:3029–42. http://dx.doi.org/10.1029/92WR01482.
[31] Marks D, Winstral A, Flerchinger G, Reba M, Pomeroy J, Link T, et al. Comparing simulated and measured sensible and latent heat fluxes over snow under a pine canopy to improve an energy balance snowmelt model. J Hydrometeorol 2008;9:1506–22. http://dx.doi.org/10.1175/2008JHM874.1.
[32] Marks D, Winstral A. Comparison of snow deposition, the snow cover energy balance, and snowmelt at two sites in a semiarid mountain basin. J Hydrometeorol 2001;2:213–27. http://dx.doi.org/10.1175/1525-7541(2001)002<0213:COSDTS>2.0.CO;2.
[33] Seyfried MS, Grant LE, Marks D, Winstral A, McNamara J. Simulated soil water storage effects on streamflow generation in a mountainous snowmelt environment, Idaho, USA. Hydrol Proc 2009;23:858–73. http://dx.doi.org/10.1002/hyp.7211.
[34] Reba ML, Marks D, Winstral A, Link TE, Kumar M. Sensitivity of the snowcover energetics in a mountain basin to variations in climate. Hydrol Proc 2011;25:3312–21. http://dx.doi.org/10.1002/hyp.8155.
[35] Winstral A, Marks D, Gurney R. An efficient method for distributing wind speeds over heterogeneous terrain. Hydrol Proc 2009;23:2526–35. http://dx.doi.org/10.1002/hyp.7141.
[36] Winstral A, Marks D. Simulating wind fields and snow redistribution using terrain-based parameters to model snow accumulation and melt over a semi-arid mountain catchment. Hydrol Proc 2002;16:3585–603. http://dx.doi.org/10.1002/hyp.1238.
[37] Kumar M, Duffy CJ, Salvage KM. A second-order accurate, finite volume-based, integrated hydrologic modeling (FIHM) framework for simulation of surface and subsurface flow. Vadose Zone J 2009;8:873–90. http://dx.doi.org/10.2136/vzj2009.0014.
[38] Kumar M, Bhatt G, Duffy CJ. An object-oriented shared data model for GIS and distributed hydrologic models. Int J Geog Info Sci 2010;24:1061–79. http://dx.doi.org/10.1080/13658810903289460.
[39] Marks D. Introduction to special section: Reynolds Creek Experimental Watershed. Water Resour Res 2001;37:2817. http://dx.doi.org/10.1029/2001WR000941.
[40] Marks D, Seyfried M, Flerchinger G. A winstral research data collection at the Reynolds Creek Experimental Watershed. J Service Climatol 2007:1–18.
[41] Nayak A, Marks D, Chandler DG, Seyfried M. Long-term snow, climate, and streamflow trends at the Reynolds Creek Experimental Watershed, Owyhee Mountains, Idaho, United States. Water Resour Res 2010;46:W06519. http://dx.doi.org/10.1029/2008WR007525.
[42] Robinson DA, Abdu H, Jones SB, Seyfried M, Lebron I, Knight R. Eco-geophysical imaging of watershed-scale soil patterns links with plant community spatial patterns. Vadose Zone J 2008;7:1132–8. http://dx.doi.org/10.2136/vzj2008.0101.
[43] Marks D, Winstral A, Seyfried M. Simulation of terrain and forest shelter effects on patterns of snow deposition, snowmelt and runoff over a semi-arid mountain catchment. Hydrol Proc 2002;16:3605–26. http://dx.doi.org/10.1002/hyp.1237.
[44] Hanson CL, Marks D, Van Vactor SS. Long-term climate database, Reynolds Creek Experimental Watershed Idaho United States. Water Resour Res 2001;37:2839–41. http://dx.doi.org/10.1029/2001WR000417.
[45] Dubayah R, van Katwijk V. . The topographic distribution of annual incoming solar radiation in the Rio Grande River basin. Geophys Res Lett 1992;19:2231–4. http://dx.doi.org/10.1029/92GL02284.
[46] Dozier J. A clear-sky spectral solar radiation model for snow-covered mountainous terrain. Water Resour Res 1980;16:709–18. http://dx.doi.org/10.1029/WR016i004p00709.
[47] Link TE, Marks D. Point simulation of seasonal snow cover dynamics beneath boreal forest canopies. J Geophys Res 1999;104:27841–58. http://dx.doi.org/10.1029/1998JD200121.
[48] Link TE, Marks D, Hardy JP. A deterministic method to characterize canopy radiative transfer properties. Hydrol Proc 2004;18:3583–94. http://dx.doi.org/10.1002/hyp.5793.

[49] Marshall SE, Warren SG. Parameterization of snow albedo for climate models. In: Goodison BE, Barry RG, Dozier J, editors. Large scale effects of seasonal snow cover, vol. 166, Intl. Assoc. Hydrol. Sci. Publ.: Wallingford, UK; 1987. pp. 43–50.
[50] Hardy JP, Melloh R, Koenig G, Marks D, Winstral A, Pomeroy JW, et al. Solar radiation transmission through conifer canopies. Agric Forest Meteorol 2004;126:257–70. http://dx.doi.org/10.1016/j.agrformet.2004.06.012.
[51] Marks D, Dozier J. A clear-sky longwave radiation model for remote alpine areas. Theory Appl Climatol 1979;27:159–87. http://dx.doi.org/10.1007/BF02243741.
[52] Byers HR. General Meteorology. 4th ed. New York: McGraw-Hill; 1974. p. 461. http://dx.doi.org/10.1002/qj.49708636716.
[53] Marks D, Winstral A, Reba M, Pomeroy J, Kumar M. An evaluation of methods for determining during-storm precipitation phase and the rain/snow transition elevation at the surface in a mountain basin. Adv Water Resour 2012. http://dx.doi.org/10.1016/j.advwatres.2012.11.012.
[54] Hanson RT, Newhouse MW, Dettinger MD. A methodology to asess relations between climatic variability and variations in hydrologic time series in the Southwestern United States. J Hydrol 2004;287:252–69. http://dx.doi.org/10.1016/j.jhydrol.2003.10.006.
[55] Pierson FB, Slaughter CW, Cram ZK. Long-term stream discharge and suspended-sediment database, Reynolds Creek Experimental Watershed, Idaho, United States. Water Resour Res 2001;37:2857–61. http://dx.doi.org/10.1029/2001wr000420.
[56] van Genuchten MT. A closed-form equation for predicting the hydraulic conductivity of unsaturated soils. Soil Sci Soc Am J 1980;44:892–8. http://dx.doi.org/10.2136/sssaj1980.03615995004400050002x.
[57] Flerchinger GN, Marks D, Reba ML, Yu Q, Seyfried MS. Roles of spatially varying vegetation on surface fluxes within a small mountainous catchment. Hydrol Earth Syst Sci 2010;14:965–78. http://dx.doi.org/10.5194/hess-14-965-2010.
[58] Reba ML, Marks D, Seyfried M, Winstral A, Kumar M, Flerchinger G. A long-term data set for hydrologic modeling in a snow-dominated mountain catchment. Water Resour Res 2011;47:W07702. http://dx.doi.org/10.1029/2010WR010030.
[59] Pomeroy JW, Toth B, Granger RJ, Hedstrom NR, Essery RLH. Variation in surface energetics during snowmelt in a Subarctic mountain catchment. J Hydrometeorol 2003;4:702–19. http://dx.doi.org/10.1175/1525-7541(2003)004<0702:viseds>2.0.co;2.